Cyclonically Forced Barrier Winds along the Transantarctic Mountains near Ross Island*

WILLIAM P. O'CONNOR†

Institute for Naval Oceanography, Stennis Space Center, Mississippi

DAVID H. BROMWICH AND JORGE F. CARRASCO@

Byrd Polar Research Center and Atmospheric Sciences Program, The Ohio State University, Columbus, Ohio

(Manuscript received 24 March 1993, in final form 13 August 1993)

ABSTRACT

The effect of the Transantarctic Mountains on cyclonically forced boundary-layer winds in the vicinity of Ross Island, Antarctica (77.5°S, 167°E), is discussed. When cyclones are present over the western Ross Ice Shelf and Ross Sea, the low-level easterly airflow is toward the mountains. A barrier wind regime is set up as the flow is turned northward and becomes parallel to the mountain range. It is found that cyclonically forced barrier winds occurred around 5% and 8% of the time during 1984 and 1985, respectively.

The case histories of two well-defined barrier wind events lasting for 24 h are discussed in detail, with regional analyses based on satellite photographs and automatic weather station data. One case is for a katabatic wind–forced mesoscale cyclone forming to the north of Ross Island, and the other is for a synoptic-scale cyclone moving through the western Ross Ice Shelf–Ross Sea region.

A numerical model for the vertically integrated boundary-layer flow that calculates two horizontal velocities and the boundary-layer depth is used to investigate the mountain barrier effect on low-level airflow. The domain is the region of the western Ross Ice Shelf–Ross Sea from 82° to 76°S, between Byrd Glacier and Terra Nova Bay, and bounded to the west by the Transantarctic Mountains. The boundary-layer airflow is constrained to remain below the height of the mountains, so that the surface airflow is around the topographic features of Minna Bluff and Ross Island. The two cases of cyclonic forcing are modeled, with the isobars intersecting the mountains obliquely. The model depicts the pressure increases and stagnation zones south of Minna Bluff and Ross Island, and the surface airflow eastward past these features, which agree with observations.

1. Introduction

Ross Island is located at the northern and western boundaries of the Ross Ice Shelf (Fig. 1). It is a volcanic island composed of three mountain peaks. At its southwestern tip is located McMurdo Station, the principal United States logistical support base for research in the Antarctic. North of Ross Island, the Ross Sea is frozen over during the austral winter but has open water in summer. The Ross Ice Shelf is a flat, smooth floating ice sheet, bounded to the west and south by the Transantarctic Mountains, a very steep mountain chain over 2000 m high. To the west of this range is the high interior plateau of the East Antarctic ice sheet. The presence of the Transantarctic Mountains 50 km to the west of Ross Island has a strong effect on the mesoscale meteorology. This article discusses the origin and dynamics of barrier wind events that occur in this region. These may result in gale-force winds at McMurdo, and the problems in forecasting them are discussed by Mullen (1987).

The dynamics of the barrier wind regime that affects Ross Island is discussed by Slotten and Stearns (1987) and O'Connor and Bromwich (1988). When cyclonically forced boundary-layer winds blow toward a high, steep topographic barrier, they can be deflected, and eventually, a barrier wind blowing parallel to the mountains is established. These winds are in geostrophic balance with the pressure gradient normal to the mountains, caused by the damming of stable air and the subsequent increase in boundary-layer depth. Examples are given by Schwerdtfeger (1984, 94–99), in which a stationary cyclone over the Ross Ice Shelf or southern Ross Sea can have its low-level winds blocked by the Transantarctic Mountains, giving rise to the strong southerly mountain parallel barrier winds approaching Ross Island.

Cyclonically forced barrier winds are not the only source of persistent southerly winds near Ross Island. Some of the southeasterly winds can be the result of

* Contribution 869 of Byrd Polar Research Center.

† Present address: NOAA Great Lakes Environmental Research Labs., Ann Arbor, MI 48105.

@ Permanent affiliation: Dirección Meteorológica de Chile, Santiago, Chile.

Corresponding author address: Dr. David H. Bromwich, Byrd Polar Research Center, Ohio State University, 108 Scott Hall, 1090 Carmack Rd., Columbus, OH 43210-1002.

geostrophic airflow associated with synoptic-scale cyclones that cross and/or decay just to the northeast of the Ross Ice Shelf (e.g. Taljaard 1972; Physick 1981; Schwerdtfeger 1984; Carleton 1992). Also, southerly and/or south-southwesterly winds can result from katabatic airstreams that propagate horizontally from Skelton, Mulock, and Byrd glaciers (Liu and Bromwich 1993) and along the Transantarctic Mountains from southern Marie Byrd Land (Bromwich et al. 1992, 1994). This article discusses in detail the modification of synoptic and mesoscale cyclones by the Transantarctic Mountains near Ross Island that leads to the development of barrier wind events. The next section outlines the basic dynamics when cyclonic winds are blocked at a topographic barrier. Section 3 presents a survey of barrier wind events for the 1984–85 period and two case studies for both a synoptic and a mesoscale cyclone passage along the Transantarctic Mountains. In section 4 a numerical model that can investigate the barrier wind dynamics is described. Finally, in section 5, the model is applied to investigate features of these two cyclone cases, and the results are discussed.

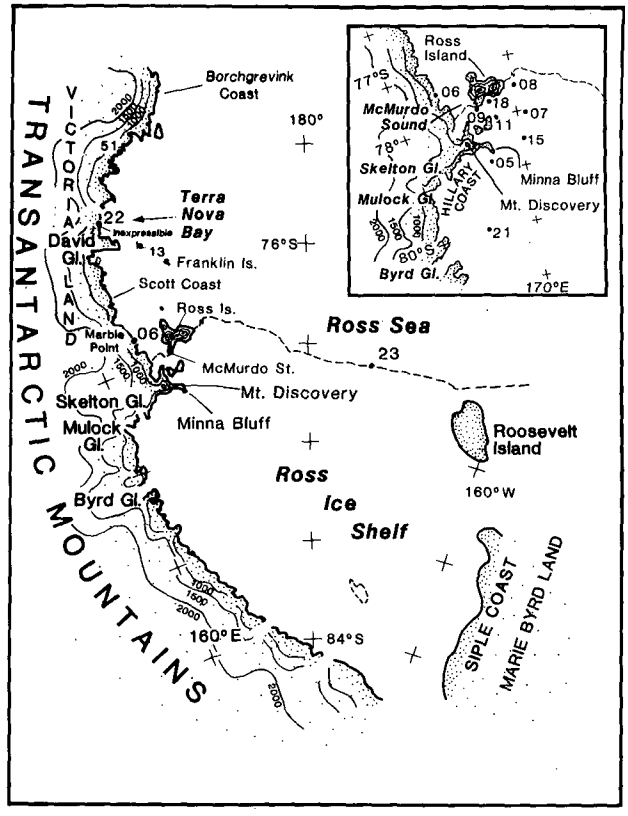

FIG. 1. Location map of the Ross Ice Shelf and surrounding area. Inset provides location of the AWS sites (dots with numbers attached) during 1984 near Ross Island. Thin solid lines are elevation contours in meters. The thin solid lines on Ross Island are elevation contours at 500-m increments starting from 1000 m.

2. Dynamics of barrier wind events

The local modification of maritime cyclones by coastal mountain ranges is known to occur at several places around the world. In high latitudes this takes place along the Brooks Range in Alaska (Kozo and Robe 1986) and the Canadian Arctic coast (Lu and Sackinger 1989). The ice plateau of Greenland can block synoptically forced easterly winds resulting in gale-force winds along the eastern coast (Hsu 1988, 163–165). Maritime cyclones direct slightly stable low-level air toward the steep coastal slopes of Antarctica, and the resulting blocking plays an important role in the orographic snowfall generation in those areas (Bromwich 1988a).

We wish to discuss the effect of orography on the low-level dynamics of a cyclone. This depends on the depth and stability of the atmospheric boundary layer and on the height of the terrain barrier. The basic physics is described by Overland (1984, 1986) and Mass and Albright (1987), who show that when a flow encounters a topographic barrier, the resulting dynamics is decided by two relevant scaling parameters: the Froude number and the Rossby deformation radius. The consideration of whether airflow will be over or around any terrain feature is best analyzed by an internal Froude number based on the height h of the terrain obstacle:

$$\mathrm{Fr} = U_0\left(gh\frac{\Delta\theta}{\theta}\right)^{-1/2}, \qquad (1)$$

where U_o is the approaching wind speed, $g = 9.8\ \mathrm{m\ s^{-2}}$, θ is the average potential temperature of this layer, and $\Delta\theta$ is the potential temperature increase of the stable stratification between the surface and the height of the obstacle. For the case $0 < \mathrm{Fr} < 1$, the air at the surface lacks the kinetic energy to flow over the obstacle, and so there will be surface airflow around it. Along the Transantarctic Mountains from Byrd Glacier to Terra Nova Bay, the mountain range rises steeply to a height of $h = 2000$ m or more (Fig. 1). During wintertime barrier wind events, the radiosonde observations at McMurdo give typical values $\theta = 260$ K and $\Delta\theta = 10$ K (O'Connor and Bromwich 1988). If we assume that cyclonically forced boundary-layer winds blowing toward the mountains have a speed of $U_o = 10\ \mathrm{m\ s^{-1}}$, the preceding formula gives a Froude number of 0.4, so that the surface airflow will be around the terrain obstacles.

The boundary-layer inversion of the Ross Ice Shelf always remains below the barrier of the Transantarctic Mountains. For stable flow conditions, the Rossby deformation radius is an e-folding scale that determines the horizontal distance to which the mountain's presence influences the cyclone dynamics:

$$R = \left(gH\frac{\Delta\theta}{\theta}\right)^{1/2}\left|\frac{1}{f}\right|, \qquad (2)$$

where f is the Coriolis parameter (-1.43×10^{-4} s^{-1}), H is the (undisturbed) depth of the boundary layer, θ is the average potential temperature of the layer, and $\Delta\theta$ is the potential temperature increase between the boundary layer and the layer above. Within this distance, the winds parallel to the mountains can be in geostrophic balance with the pressure gradient normal to the mountains. The winter boundary-layer conditions at McMurdo are typically H = 1000 m, θ = 260 K, and $\Delta\theta$ = 8 K. These conditions give a Rossby deformation radius of about 121 km, within which the mountains can exert a strong topographic control.

3. Observational study of cyclonically forced barrier winds near Ross Island

Recent observational studies (e.g., Bromwich 1991; Carrasco 1992; Carrasco and Bromwich 1993) have shown that the southwestern corner of the Ross Sea near Terra Nova Bay is a cyclogenetic area where one or two mesoscale cyclones form each week throughout the year. These studies made use of data from an array of automatic weather stations (AWS) deployed around the region (Fig. 1, Savage et al. 1985). When a mesoscale cyclone moves toward Ross Island, the circulation can affect the northwestern side of the Ross Ice Shelf by supporting northeasterly to easterly winds blowing perpendicular to the mountains. The same circulation can be set up by synoptic-scale cyclones entering the Ross Sea–Ross Ice Shelf area from the north and east (Bromwich 1986, 1988b). This situation can create conditions for the development of barrier winds (Schwerdtfeger 1984). A two-year survey of barrier wind events is presented in section 3a, and two case studies of cyclonically forced barrier wind events are described in sections 3b and 3c. The first case is associated with a subsynoptic-scale cyclone located to the east of Ross Island, and the second is linked to a synoptic-scale cyclone that crossed the Ross Ice Shelf from the east.

a. Two-year study of barrier wind events

A survey of cyclonically forced barrier wind events over the northwestern side of the Ross Ice Shelf was carried out for the period February 1984–December 1985 in order to determine their frequency and duration; the AWS array for this period provided a good description of the pressure field between Minna Bluff and the south side of Ross Island (Fig. 1). The mesoscale analyses constructed twice daily (0000 and 1200 UTC) by Bromwich (1991) from AWS observations and satellite imagery during the above period were examined. The frequency was calculated by counting all the charts that showed 1) surface isobars at a large angle to the Transantarctic Mountains over the northwestern Ross Ice Shelf, and 2) wind directions normal to the isobars as observed by AWS sites deployed in that area. (Figures 5 and 10 introduced later provide examples.) Also, the wind speed was required to be stronger than the monthly average. Because the analyses were made every 12 h, it was assumed that one analysis represents the average regional conditions within ±6 h of the actual analysis time (0000 and 1200 UTC). Thus, if the above conditions were met for one (two) chart(s), then the event had a duration of 12 (24) h. In reality, one chart may represent an event of a few minutes to nearly 24 h in duration; however, for simplicity the preceding assumption was adopted for our analysis.

Table 1 shows the total number of monthly events (N) for 1984 and 1985. It reveals that around 11% and 7% of the time the northwestern Ross Ice Shelf was affected by barrier winds in 1984 and 1985, respectively. About 41% and 42%, respectively, of the total annual events (32 for 1984, and 24 for 1985) were found on only one chart indicating that the duration of these events was 12 h. Restricting the first requirement to those cases that showed cyclonic isobars oriented at a large angle to the Transantarctic Mountains, it is found that 67% (22 events out of 32) and 92% (22 events out of 24) of the total events can be classified as true cyclonically forced barrier winds in 1984 and 1985, respectively. The inertial period at 79°S is 12.2 h. This is an approximate scale for the time it takes the airflow to reach steady-state geostrophic conditions for barrier wind events. Therefore, it is assumed that only the cases that were analyzed on two or more consecutive charts are well-developed barrier wind events, so that they represent events with a duration of at least 24 h. The monthly number n of these cases is given in Table 1. About 59% and 58% of the total events lasted one or more days in 1984 and 1985, respectively. From the total of these cases, about 74% in 1984 and 93% in 1985 were cyclonically forced barrier wind events. They

TABLE 1. Number of monthly barrier wind events for 1984 and 1985; N (CF) indicates the total number of events (cyclonically forced events), and n (cf) denotes the total number of events (cyclonically forced events) with duration of more than 12 h.

	1984				1985			
Month	N	CF	n	cf	N	CF	n	cf
January	—	—	—	—	0	0	0	0
February	4	4	3	3	2	2	2	1
March	3	3	2	2	2	1	1	1
April	2	2	2	2	3	2	1	1
May	4	3	1	1	2	2	2	2
June	5	2	4	2	3	3	1	1
July	4	3	3	2	2	2	2	2
August	3	2	1	0	2	2	1	1
September	3	0	0	0	3	2	1	1
October	3	2	2	2	3	2	3	2
November	1	0	1	0	2	2	0	1
December	0	0	0	0	0	0	0	0
Annual	32	22	19	14	24	22	14	13

constitute around 8% and 5% of the time during 1984 and 1985, respectively. Note that no such events took place in December 1984, January 1985, and December 1985. These months correspond to the austral summer season in Antarctica when the boundary-layer stratification is weakest (O'Connor and Bromwich 1988). Figure 2 shows the frequency distribution of the cyclonically forced events that lasted one or more days. Also the percentage of the events that were analyzed only on one chart and the actual number of events are included. The results indicate that around 50% (7 out of 14) and 85% (11 out of 13) of the cyclonically forced events in 1984 and 1985, respectively, had a duration of less than two days.

b. *Mesoscale cyclogenesis case study*

The first case occurred from 20 to 23 February 1984 and was initially studied by Bromwich (1987). The appropriate conditions for barrier wind formation resulted from a pair of mesoscale cyclones, one located just to the east of Ross Island and the other near Franklin Island. They established cyclonically forced boundary-layer winds blowing toward the Transantarctic Mountains. The regional analysis at 0000 UTC 21 February (Fig. 3) shows three cyclonic features. The 3-h AWS analyses resolved a mesoscale cyclonic circulation (L_1 in Fig. 3) over the southwestern Ross Sea at 0900 UTC 20 February. Available Defense Meteorological Satellite Program (DMSP) satellite images at

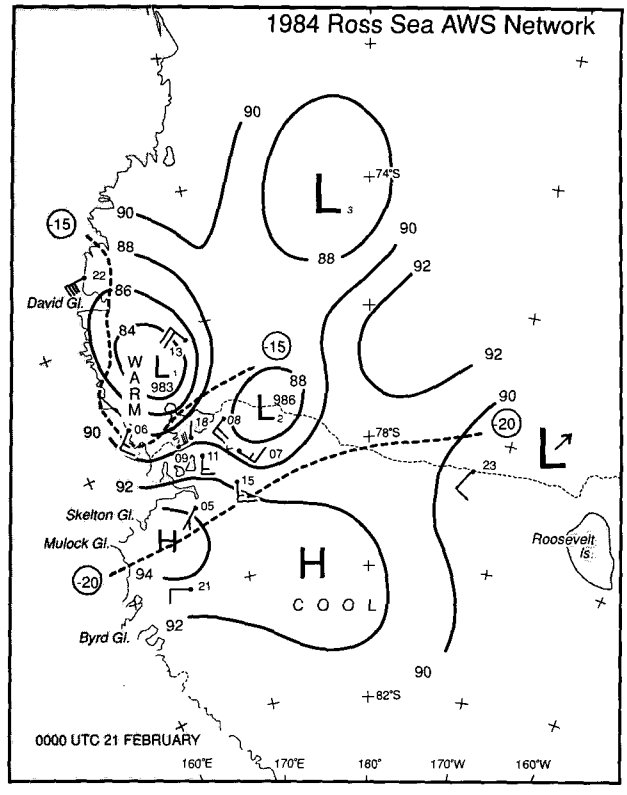

FIG. 3. Regional analysis of the sea level isobars (hPa, solid, 88 = 988) and surface isotherms (°C, dashed) from AWS observations at 0000 UTC 21 February 1984.

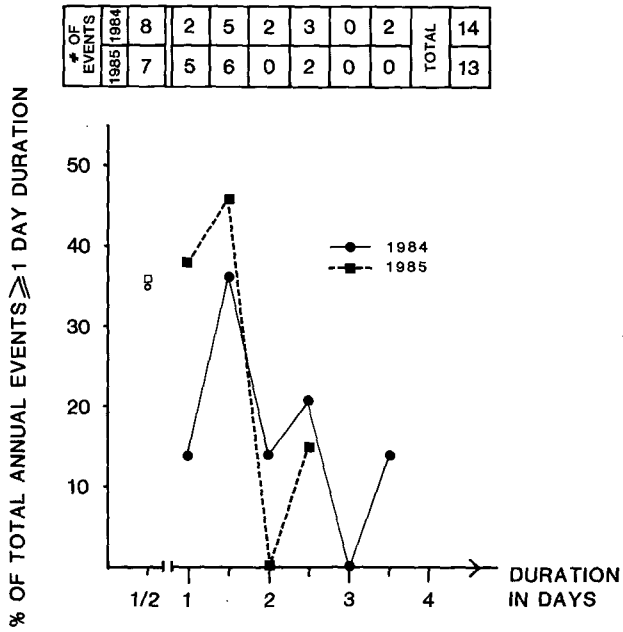

FIG. 2. Frequency distribution of cyclonically forced barrier wind duration (24 h or more) for 1984 and 1985. The number of events is listed above the duration. The open circle and square are percentages of events on only one chart with respect to the total numbers of events.

0104 and 0221 UTC 21 February show a weak cloud signature that was associated with this mesoscale cyclone. Unfortunately, the quality of the available hardcopy satellite images is not good enough for reproduction; however, for reference, a schematic illustration of the main features of the latter image is given in Fig. 4. The DMSP images also revealed another mesoscale cyclone (L_2 in Figs. 3 and 4) located just to the east of Ross Island and a third cyclonic cloud-shaped structure (L_3 in Figs. 3 and 4) located to the northeast of Franklin Island. The latter was the largest of the three cyclones but still within the subsynoptic scale (less than 1000 km in diameter), and according to the Australian synoptic analyses, it seems to be the remnant of a synoptic-scale system that approached the area. At this time, the pressure field already indicates geostrophic airflow almost perpendicular to the Transantarctic Mountains over the northwestern corner of the Ross Ice Shelf.

A sequence of DMSP satellite images at 0542, 0702, 1830, and 2358 UTC 21 February indicates that the subsynoptic cyclone (L_3) moved toward the south and was located to the east of Ross Island at 1830 UTC 21 February. During this time, the Ross Ice Shelf mesoscale cyclone (L_2) remained almost stationary to the east of Ross Island and appeared to merge with cyclone L_3 around 2100 UTC 21 February. Meanwhile, the

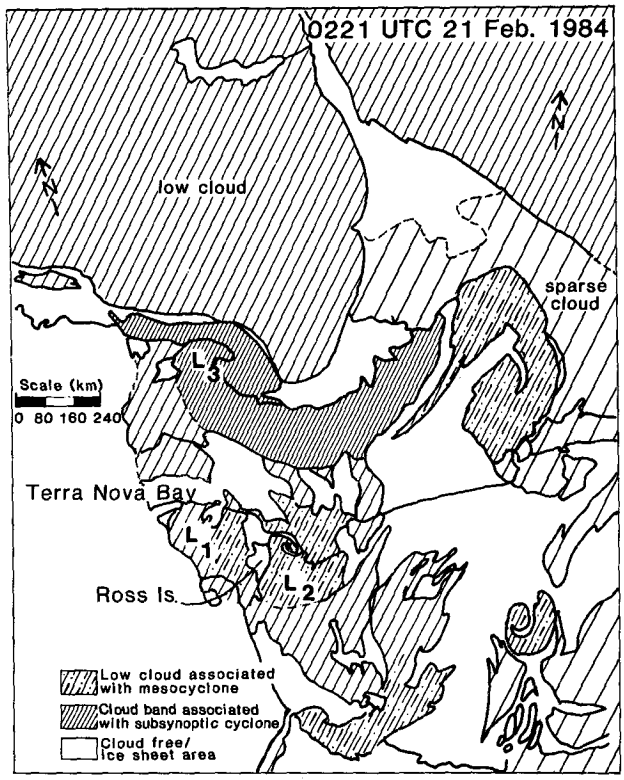

FIG. 4. Schematic of a DMSP visible satellite image at 0221 UTC 21 February 1984.

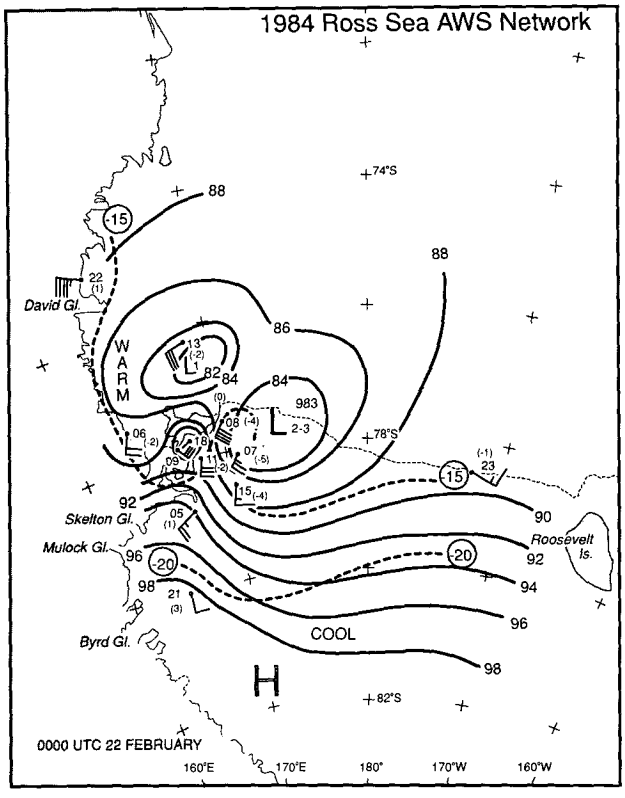

FIG. 5. Same as Fig. 3 but at 0000 UTC 22 February 1984. Pressure changes (hPa) during the preceding 24 h are given in parentheses next to each AWS site.

first mesoscale cyclone (L_1) remained nearly stationary in the vicinity of Franklin Island where it dissipated slowly after 1200 UTC 22 February. The 3-h analyses revealed that as mesoscale cyclone L_3 moved southward the pressure gradient over the Ross Ice Shelf increased. Figure 5 shows the AWS analysis at 0000 UTC 22 February, while Fig. 6 is the schematic representation of the DMSP image at 0407 UTC 22 February showing the position of the mesocyclone L_1 and the combined subsynoptic cyclone L_2–L_3. Note that the sea level pressure difference between AWS 07 and AWS 05 had increased from 4 to 10 hPa over the last 24 h. At this time, the combined cyclone (L_2 and L_3) is located to the east of Ross Island and the mesoscale cyclone L_1 to the south of Franklin Island (see Fig. 6).

The geostrophic circulation inferred from the sea level pressure analysis shows stronger airflow blowing toward the Transantarctic Mountains (compare Figs. 3 and 5). This cyclonic circulation probably brought stable boundary-layer air toward the mountains where it was dammed up by the orography. The pressure tendencies during the last 24 h indicate greater decreases of the pressure at those stations located farther away from the mountains (AWS 15, 07 and 08) than those located immediately to the east of them (AWS 11 and 18). Also, pressure increases took place at AWS 05 and 21. The behavior of these pressure tendencies can be associated with the damming up of stable air by the mountains (Parish 1983). If this is the case, the damming of stable air creates a pressure gradient perpendicular to the topographic barrier. Eventually, a barrier

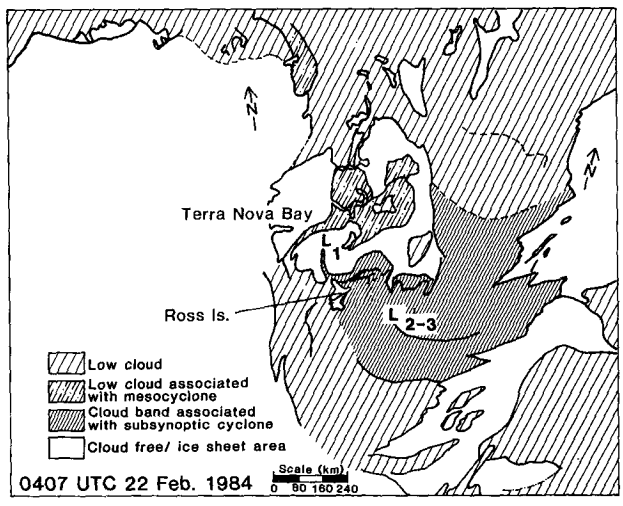

FIG. 6. Same as Fig. 4 but at 0407 UTC 22 February 1984.

wind regime is set up, where the winds are in geostrophic balance with this pressure gradient. This situation seems to be present at 0000 UTC 22 February as the surface winds parallel to the mountains significantly increased sometime between 1800 and 2100 UTC 21 February.

The subsequent satellite images at 0319, 0407, 0459, 0703, 1023, and 1838 UTC 22 February show that both cyclones remained nearly stationary. The DMSP image at 1023 UTC showed disorganized cloud signatures indicating only one cyclonic circulation over the southwestern Ross Sea, but the regional analysis at 1200 UTC 22 February still resolved both cyclones. At this time, the combined mesoscale cyclone (L_2 and L_3) had moved to the north of its earlier position at 0000 UTC 22 February (Fig. 5). The counterclockwise rotation of the wind at Franklin Island between 0300 and 0600 UTC 22 February indicates that the mesoscale cyclone L_1 moved toward the northeast. Also, the regional analysis showed that a nearly stationary sea level pressure field affected the Ross Ice Shelf during this period, supporting the continuation of the barrier winds. A gradual decrease of the surface winds and the pressure gradient over the Ross Ice Shelf suggests that the barrier wind event ended around 2100 UTC 22 February, although some manifestation was still present around Ross Island until 0300 UTC 23 February. Figure 7 shows the pressure field at 0000 UTC 23 February. At this time the analysis resolved only a cyclonic center to the northeast of Franklin Island indicating that both systems had combined. This circulation remained stationary over the area and completely dissipated by 0000 UTC 25 February.

As mentioned above, at 0000 UTC 21 February (Fig. 3) a cyclonic circulation associated with a mesoscale cyclone (L_2) already directed the airflow perpendicular to the mountains over the northwestern corner of the Ross Ice Shelf. At this time, the wind speed at AWS 08 was already above its monthly average but a significant increase occurred around 1800 UTC 21 February. Other significant increases of wind speed, above the monthly average, took place at AWS 05 and 11 at 2100 UTC 21 February and 0000 UTC 22 February, respectively. These increases occurred around the time when the mesoscale cyclone L_2 and the subsynoptic cyclone L_3 merged just to the east of Ross Island, creating the appropriate conditions for the barrier wind event at 2100 UTC 21 February. The large increase of wind speed at AWS 05 can signal the initiation of the barrier winds. This suggests that the barrier wind event occurred almost immediately after establishment of the pressure field with isobars perpendicular to the mountainous terrain. Winds were back to their respective monthly averages after 24 and 30 h at AWS 05 and 11, which suggests a duration of 24–30 h. The appropriate conditions for barrier winds remained until 0000 UTC 24 February, although they started to weaken after 0000 UTC 23 February.

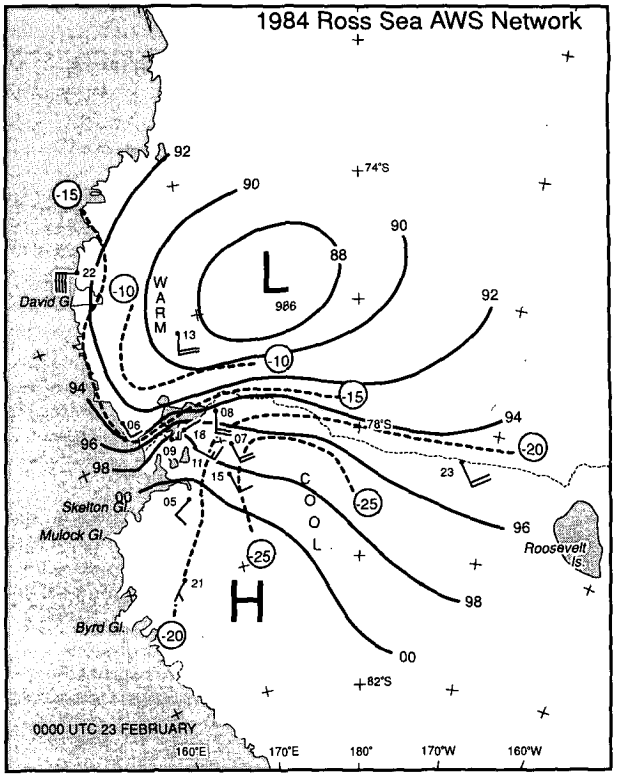

FIG. 7. Same as Fig. 3 but at 0000 UTC 23 February 1984.

c. *Synoptic cyclone case study*

According to the sea level pressure analyses produced by the Australian Bureau of Meteorology, a synoptic-scale cyclone crossed the Ross Ice Shelf–Ross Sea sector between 0000 UTC 14 April and 0000 UTC 17 April 1984. This created a pressure field where the isobars were aligned at an acute angle to the Transantarctic Mountains (Bromwich 1986). Figure 8 is the regional AWS analysis at 0000 UTC 15 April. It shows that the isobars are aligned almost parallel to the mountains to the west and north of Ross Island but are perpendicular to the Hillary Coast. Note the strong northwesterly winds at AWS 22, 13, and 08. They represent a katabatic outflow from Terra Nova Bay. Further discussion of this event is given by Bromwich (1986). The sketch from the DMSP satellite image at 0430 UTC 15 April (Fig. 9) showed a cyclonically shaped low cloud signature over the southwestern corner of the Ross Sea, suggesting a northward displacement of the cyclone. This is confirmed by the 3-h regional analyses that placed the cyclone just to the north of Franklin Island with a pressure of about 957 hPa at 1200 UTC 15 April. The general increase of the sea level pressure over the Ross Ice Shelf after 0300 UTC and the abrupt termination of the katabatic winds from Terra Nova Bay between 0600 and 0900 UTC 15 April (Bromwich 1986) also confirm this movement.

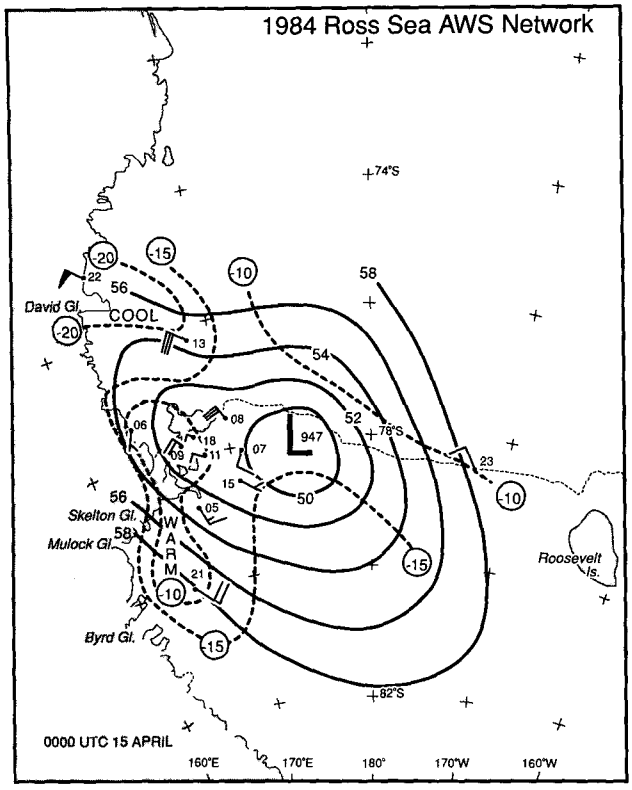

FIG. 8. Same as Fig. 3 but at 0000 UTC 15 April 1984.

A high pressure system approaching from the southeastern part of the Ross Ice Shelf was shown by the AWS analyses from 1500 UTC 15 April. At 0000 UTC 16 April, it affected the area southward of latitude 80°S. At this time, the cyclone was located just to the northeast of Franklin Island. This new location created a cyclonic circulation where easterly or southeasterly geostrophic winds blew toward Minna Bluff, the eastern side of Ross Island, and Scott Coast; southerly winds affected the southwestern corner of the Ross Sea. This circulation was restricted to the northwestern corner of the Ross Ice Shelf by the high pressure area affecting the southern part of the ice shelf. At 1200 UTC 16 April (Fig. 10) the synoptic-scale cyclone remained just to the northeast of Franklin Island. At this time, the pressure gradient over the Ross Ice Shelf–Ross Sea area had significantly increased and the cyclonic circulation seems to have extended southward as the high pressure area moved westward. The strengthening of the pressure gradient is shown by the sea level pressure difference between AWS 21 and Franklin Island, which was 9.6 hPa at 0000 UTC and 19.1 hPa at 1200 UTC 16 April. Also, the sea level pressure difference between Inexpressible and Franklin islands increased from 4.0 to 7.5 hPa. These changes are associated with the nearly stationary cyclone over the western Ross Sea and the high pressure area over the Ross Ice Shelf. Note that the positive pressure tendencies (last 12 h) of the AWS

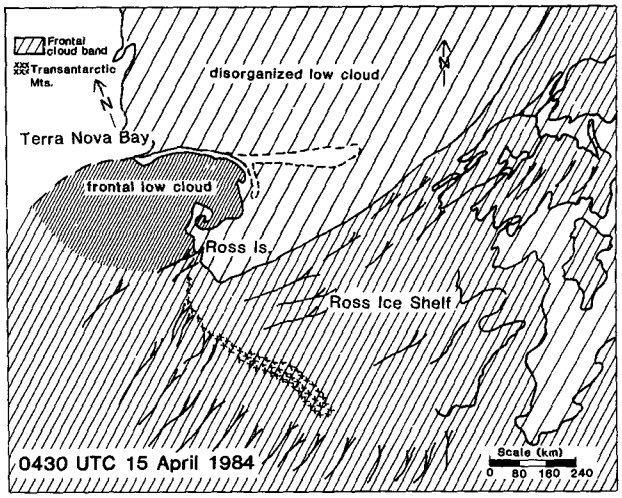

FIG. 9. Same as Fig. 4 but at 0430 UTC 15 April 1984.

sites closer to the mountains are greater than those located farther east (Fig. 10). At 1200 UTC 16 April, the pressure field had the isobars aligned obliquely to the mountains over the northwestern side of the Ross Ice Shelf (at 45° to the Hillary Coast). In this situation, the winds measured by the AWS had significantly in-

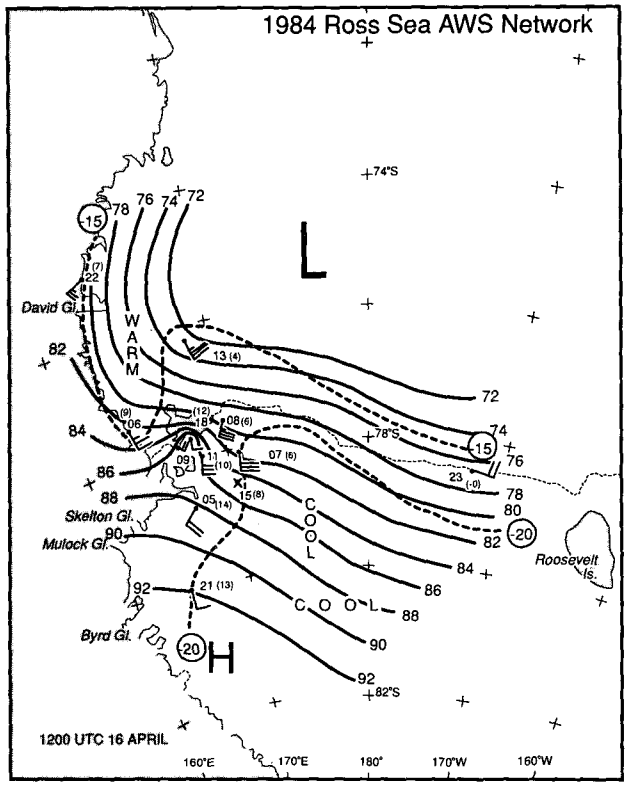

FIG. 10. Same as Fig. 3 but at 1200 UTC 16 April 1984. Pressure changes during the preceding 12 h are given in parentheses next to each AWS site.

creased by 7–12 m s^{-1} on average during the last 12 h with a southerly direction almost parallel to the Transantarctic Mountains. Once again, in this case the synoptic-scale cyclonic circulation probably directed stable boundary-layer air against the mountains. The greater increase of the pressure recorded by the AWS sites deployed immediately to the east of the mountains may be a consequence of the mountain blocking of this stable air.

The Australian analyses suggest that another dissipating storm moved into the Ross Sea on 16 April, combining with the first cyclone. However, the regional analysis at 0000 UTC 17 April indicates that the pressure gradient across the Ross Ice Shelf–Ross Sea area had decreased. The cyclonic circulation with isobars intersecting the mountains persisted over the area but the intensity of the southerly winds had also decreased. Over the next 12 h the combined system moved toward the northeast creating a subsequent pressure field where the isobars were aligned almost parallel to the mountains as the analysis at 1200 UTC 17 April revealed. Thus, according to the 3-h AWS analyses, the appropriate pressure field for barrier winds was present from about 0000 UTC 16 April until 0000 UTC 17 April. Wind speeds above the monthly average occurred between 0600 UTC 16 April and 0600 UTC 17 April at AWS 08, between 0600 UTC and 1800 UTC 16 April at AWS 11, and between 1200 UTC 16 April and 0000 UTC 17 April at AWS 05. This suggests a lag of 6–12 h between setup of easterly geostrophic flow toward the mountains and a barrier wind response, and a barrier wind duration of about 24 h.

4. The dynamical model

We wish to model the topographic influences on the mesoscale boundary-layer winds over the ice shelf for a given cyclonic forcing. The Transantarctic Mountains present a wall to the stratified boundary layer, so that the topography enters the model domain only at the position of the western boundary. This describes the surface airflow that goes around, rather than over, the high steep terrain of the Transantarctic Mountains and Ross Island. This is a departure from most studies of airflow over complex terrain and, strictly speaking, is a study of airflow around a complex boundary, but will adequately model barrier wind conditions. The simplest primitive equation model that can adequately represent the mesoscale dynamics of a mountainous coastal region is a one-layer vertically integrated model representing a stable boundary layer (Mass and Dempsey 1985, p. 1212). This should be a good approximation over the ice shelf in winter. The model does not include any diabatic effects, such as the heat flux between the surface and the boundary layer. In winter over the ice shelf the radiation inversion will still be present during synoptic events. Over the open ocean (as in the first case) the surface heat flux can be considerable and can alter the stability of the air mass (Allison et al. 1982). However, we wish to model the dynamics over the permanent ice shelf south of Ross Island. In a cyclonically forced barrier wind event we would expect weakly stratified conditions, so that the boundary-layer winds and potential temperatures are nearly constant in the vertical. The depth of the boundary layer is assumed to have the constant value 1000 m in the absence of motion. The stable stratification is modeled as a discontinuous jump (increase) in potential temperature at the top of the boundary layer. This is an oversimplification of the real conditions but is the most direct way to model the dynamics of the colder boundary-layer air over the ice shelf.

a. Equations of motion

The model uses the vertically integrated equations of motion to study the planetary boundary layer over a mesoscale domain. The four prognostic variables are the depth-averaged eastward $U(x, y, t)$ and northward $V(x, y, t)$ velocities, the boundary-layer depth $D(x, y, t)$, and the potential temperature $\theta(x, y, t)$. The flux form of the equations of motion is used because of the conservative properties in finite differencing. The horizontal momentum equation in the x direction is

$$\frac{\partial}{\partial t}(UD) + \frac{\partial}{\partial x}(U^2D) + \frac{\partial}{\partial y}(UVD) = -|f|DV - \frac{\theta}{\theta_0}D\frac{\partial}{\partial x}\left(\frac{P}{\rho}\right) - g\left(\frac{\theta_0 - \theta}{\theta_0}\right)D\frac{\partial D}{\partial x} + \frac{1}{2}D^2\frac{g}{\theta}\frac{\partial \theta}{\partial x} - C_D U(U^2 + V^2)^{1/2}, \quad (3)$$

and an analogous momentum equation can be written in the y direction.

In the preceding equation the first term on the left is the local time derivative. The next two terms are the nonlinear advective accelerations, which are important in the balance of forces close to a topographic boundary. The first term on the right is the Coriolis acceleration, deflecting airflow to the left in the Southern Hemisphere. The next three terms on the right are the result of the vertically integrated pressure gradient (Lavoie 1972; Keyser and Anthes 1977). The first of these is the pressure gradient above the boundary layer, which forces the boundary-layer winds over the ice shelf. This pressure field $P(x, y)$ will be specified as a stationary cyclone. A representative density for the boundary layer is $\rho = 1.2$ kg m^{-3}. The next term is the restoring force due to the stratification. It is the pressure gradient force introduced by the displacement of the boundary-layer height from the horizontal, resulting from the boundary-layer airflow being dammed up against the topography. The next term is the pressure gradient due to horizontal changes in lower-layer temperature (and hence density). The last term gives the

surface frictional deceleration with a quadratic resistance law. The coefficient of surface friction over a flat smooth ice surface has a representative value of $C_D = 1.5 \times 10^{-3}$ (Overland 1985). Any frictional stress at the top of the boundary layer is neglected. The continuity equation for the boundary-layer flow is

$$\frac{\partial D}{\partial t} + \frac{\partial}{\partial x}(DU) + \frac{\partial}{\partial y}(DV) = 0, \qquad (4)$$

and a similar equation can be written for the conservation of potential temperature in flux form.

b. *Finite-difference model*

The numerical model is that used by Overland et al. (1979, 1983) and Wilczak and Glendening (1988); the flux form of the finite-difference equations on the Arakawa C grid is integrated, using forward–backward time differencing (Haltiner and Williams 1980, 143–144) with upstream spatial differencing for the advective derivatives (Haltiner and Williams 1980, 130–131) and centered differencing elsewhere. The friction terms are lagged one time step for computational stability. The model domain ranges in latitude from 82° to 76°S, covering a region from south of Byrd Glacier to just south of Terra Nova Bay (Fig. 1). The western boundary of the domain corresponds to 160°E. We use a Cartesian coordinate system with x increasing eastward and y increasing northward. The domain extends 445 km in the x direction and 667 km in the y direction. The grid spacing is $\Delta x = \Delta y = 9.27$ km, so that the domain has 48×72 grid points. The spatial scale of the domain is enough to represent the synoptic pressure forcing, and the grid size adequately resolves the region within one Rossby deformation radius (120 km) of the Transantarctic Mountains. A time step of $\Delta t = 60$ s is adequate to ensure computational stability. The topography is used only to define the western boundary of the ice shelf, which roughly corresponds to the 1000-m elevation contour. The computations are performed over the entire domain and then set to zero over the mountainous terrain. This procedure necessitates the use of a Shapiro (1970) filter over the ice shelf region to prevent boundary effects from causing instabilities that propagate inward.

This approach is justified by the flatness of the ice shelf and the steepness of the Transantarctic Mountains, where the terrain usually rises from the ice shelf near sea level to a height of 1000 m, and often to 2000 m, over typical distances of 10–20 km (one or two grid spaces). This step topography is justified dynamically because this narrow region of mountain slope is small compared to both the scale of the synoptic forcing and the region of adjustment normal to the mountain range determined by the Rossby deformation radius. Furthermore, we are modeling cases of stable stratification where the surface air lacks the kinetic energy to flow over the mountains. During these barrier wind events, the surface winds (if not the winds higher aloft) blow parallel to the mountains, as evidenced by AWS observations.

Numerical models on mesoscale domains are critically dependent on the boundary conditions. At the mountain topography, the boundary condition is that the normal component of velocity vanishes. The southern boundary is an inflow boundary, and the temperature will be held fixed. The northern boundary is an outflow boundary, and the temperature there will be set equal to the value at the first interior point (zero normal gradient condition). The eastern boundary is located far enough from the mountains so that the boundary-layer dynamics are not influenced by the topography. The boundary-layer depth at the eastern boundary is held constant ($D = 1000$ m). Along the eastern boundary, we shall assume zero normal gradient conditions on U, V, and θ, so that these variables are determined by the large-scale synoptic forcing through the balance of forces at the interior points. This causes the model to have strongest winds along the eastern boundary, because the boundary-layer depth does not adjust to the cyclonic forcing. However, changes in boundary-layer depths near the western boundary are caused by the influence of the topography. Appropriate radiation open boundary conditions must be specified on the northern and southern boundaries to allow waves generated along the mountains to propagate out of the model domain:

$$\frac{\partial \phi}{\partial t} \pm c\frac{\partial \phi}{\partial y} = 0, \qquad (5)$$

where the gravity wave speed is

$$c = \left(gH\frac{\theta_0 - \theta}{\theta}\right)^{1/2} \qquad (6)$$

and $\phi = U$, V, and D at the northern (+) boundary and $\phi = U$ and V at the southern (−) boundary. It is necessary to hold the boundary-layer depth constant ($D = 1000$ m) along the southern boundary to obtain a stable interior solution. Because this boundary is removed from strongest synoptic forcing near Ross Island, this requirement still allows realistic results.

5. Model results and discussion

In this model the cyclonic forcing is not influenced by the presence of the mountains. This is an oversimplification of cyclone dynamics but can be used to see the effect of the mountain barrier on low-level winds. The cases we examine are relatively well-developed barrier wind regimes where the cyclonic forcing was nearly stationary for 24 h or more. The forcing was spun up over one day to reduce transient waves, and the model boundary-layer winds and height fields were stable after this time. The model was initialized with

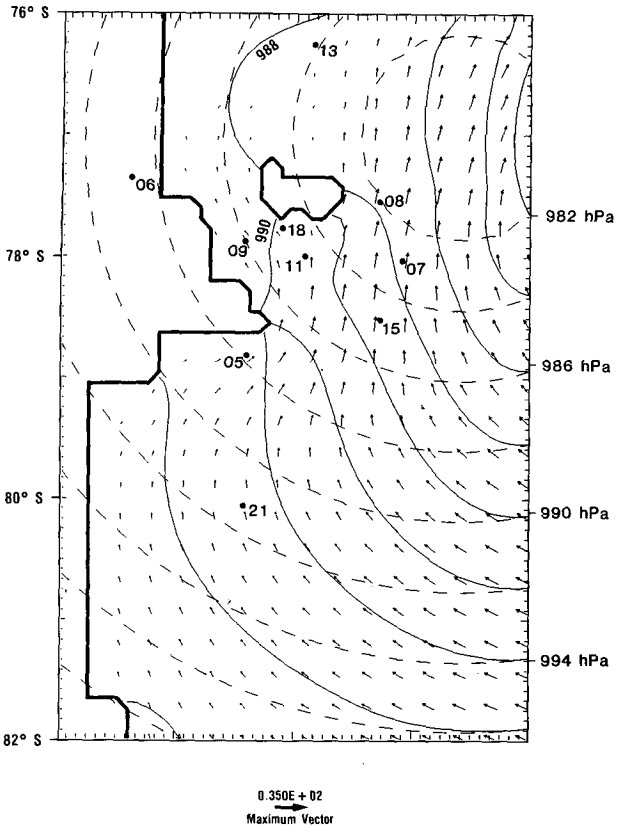

FIG. 11. Simulated resultant pressure field (solid lines) and average winds (m s^{-1}) determined by the model for the imposed pressure field (dashed lines) observed at 0000 UTC 22 February 1984. Dots with attached numbers identify locations of AWS sites.

a temperature field that varied from $\theta = 253$ K (−20°C) at the southern boundary to $\theta = 258$ K (−15°C) at the northern boundary.

a. Model cases

Two cases were selected as being representative of periods when the cyclonic pressure gradient isobars (indicating conditions above the boundary layer) had a definite orientation with respect to the Transantarctic Mountains. The first case shows cyclonic forcing isobars $P(x, y)$ (dashed lines in Fig. 11) and roughly corresponds to the time period 0000 UTC 22 February 1984 (Fig. 5). The change in the imposed sea level pressure due to the change in boundary-layer depth can be represented by the expression

$$\Delta p = \rho g \frac{\Delta\theta}{\theta}(D - 1000 \text{ m}), \qquad (7)$$

and an increase in depth of 400 m causes a pressure increase of approximately 2 hPa. The resultant surface pressure measured by the AWS is the sum of the cyclonic pressure forcing and the pressure due to the change in boundary-layer depth induced by the cyclonic forcing. This resultant surface pressure is shown in Fig. 11. The airflow is constrained to go around terrain obstacles, and the stagnation zones south of Ross Island and Minna Bluff are evident. The model results show that north of Ross Island there is a lowering of the boundary-layer height as a downstream wake effect, and there is downgradient flow toward lower pressure through McMurdo Sound. Note that the sea level pressure along the simulated barrier is increased, as the air is dammed up and geostrophic flow results.

Comparisons between the observed and simulated wind directions, wind speeds, and resultant sea level pressures are given in Table 2 for selected AWS sites located over the northwest Ross Ice Shelf. The observed data correspond to those recorded by the AWS at 0000 UTC 22 February, and the simulated data were directly estimated from the model output (Fig. 11, for the first case and Fig. 12 for the second). The comparison shows that in general the model adequately simulated the south and south-southeasterly wind directions and the overall average wind speed in the region, as well as the northward increase of the wind speed in the area just to the east of Minna Bluff and Ross Island. The largest bias is observed at AWS 13, probably due to the po-

TABLE 2. Comparison between observed and simulated wind directions, wind speeds, and resultant sea level pressures for selected AWS sites at 0000 UTC 22 February 1984.

	Wind direction/wind speed (m s^{-1})			Sea level pressure (hPa)		
AWS	Observed	Simulated	Difference (S − O)	Observed	Simulated	Difference (S − O)
08	234°/21	190°/16	−44°/−5	984.3	987.7	+3.4
07	225°/12	190°/16	−35°/+4	983.9	987.5	+3.6
15	180°/8	190°/16	+10°/+8	987.5	989.0	+1.5
13	264°/15	200°/4	−64°/−11	983.5	987.0	+3.5
11	203°/15	180°/12	−23°/−3	988.2	991.0	+2.8
05	238°/13	230°/10	−8°/−3	994.0	994.7	+0.7
21	198°/5	170°/8	−28°/+3	998.1	994.7	−3.4
Average			−27°/−1.0			+1.8
			−21°/+0.7*			+1.4*

* Average without AWS 13.

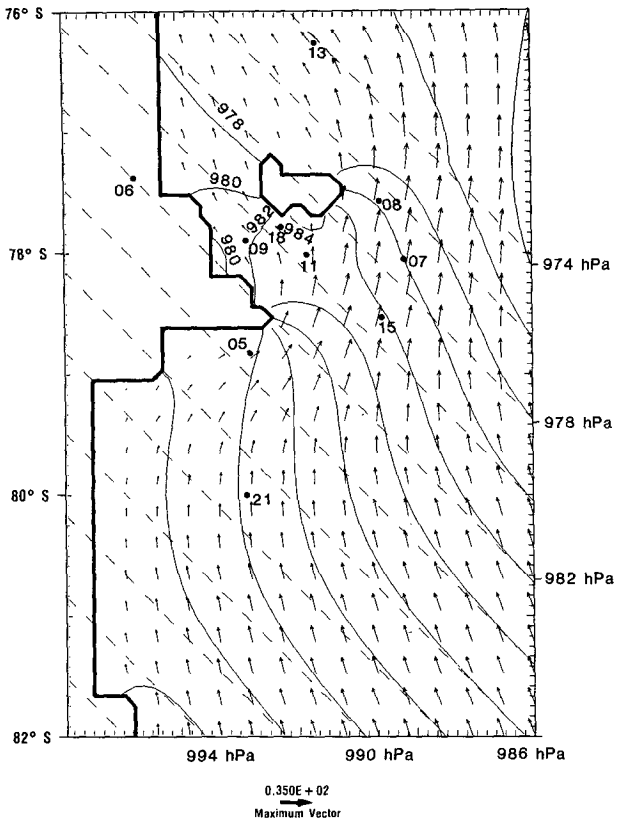

FIG. 12. Same as Fig. 11 but at 1200 UTC 16 April 1984.

sition of this station with respect to the simulated subsynoptic cyclone. Both the model and the observations show a stagnation zone south of Ross Island. The simulated sea level pressure field (solid lines in Fig. 11) suggests a low pressure center to the east-northeast of Ross Island that almost coincides with the cyclone resolved by the mesoscale analysis at 0000 UTC 22 February. Figure 13a shows the spatial differences between the simulated and observed sea level pressures at 0000 UTC 22 February (see also Table 2). It can be seen that the model simulated lower (higher) pressures than observed to the south (north) of AWS 05.

The second case shows synoptic-forcing isobars oriented at an acute angle to the Transantarctic Mountains (Fig. 12) and represents the time 1200 UTC 16 April 1984 (Fig. 10). Again, the salient features are the increased sea level pressure and stagnation zones caused by topographic blocking south of Ross Island and Minna Bluff and the downgradient flow toward lower pressure in McMurdo Sound. The observed and simulated wind speeds, wind directions, and resultant sea level pressures are given in Table 3 for 1200 UTC 16 April. Once again, the overall wind directions and resultant sea level pressure almost concur with the observed wind directions and pressure field over the northwestern side of the Ross Ice Shelf (compare Figs. 10 and 12). However, the wind speeds are overestimated in this case (Table 3). This overestimation can be explained by the fact that the model gives an integrated vertical average wind of the simulated boundary layer, while AWS record the wind just 3 m above the ice surface. Note that in the first case (Table 2) the model overestimated the wind speed for only four stations. This is probably due to stronger geostrophic airflow associated with the synoptic-scale cyclone. The spatial sea level pressure differences between the simulated and observed data are given in Fig. 13b. In this case the model simulated lower pressure values than

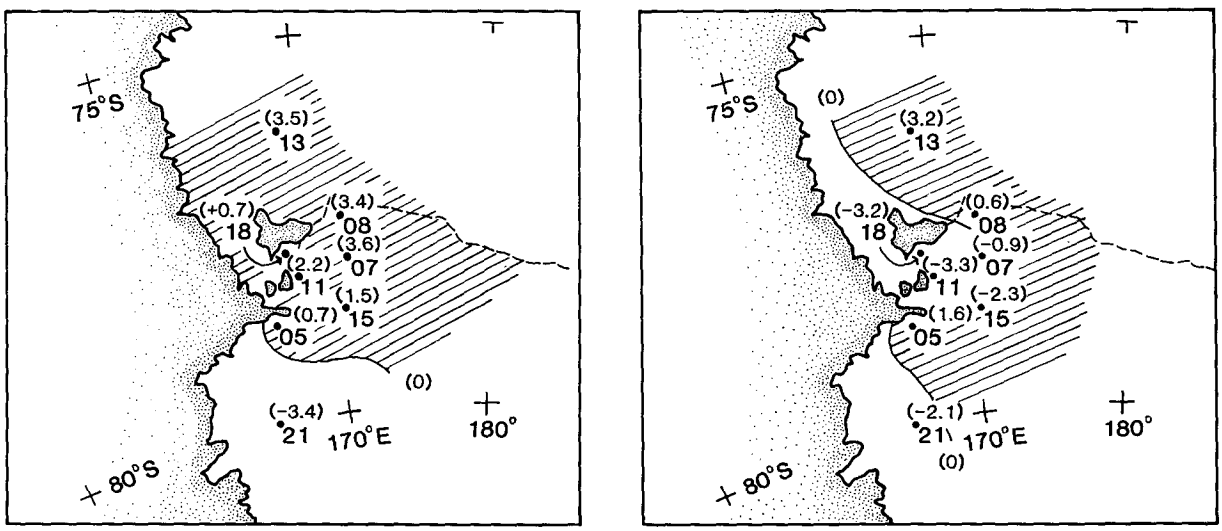

FIG. 13. Differences between simulated and observed sea level pressure at AWS 13, 18, 11, 05, 21, 08, 07, and 15 at (left panel) 0000 UTC 22 February 1984 and (right panel) 1200 UTC 16 April 1984. Shaded area defines the region where the simulated sea level pressures are higher than the observed data.

TABLE 3. Comparison between observed and simulated wind directions, wind speeds, and resultant sea level pressures for selected AWS sites at 1200 UTC 16 April 1984.

	Wind direction/wind speed ($m\ s^{-1}$)			Sea level pressure (hPa)		
AWS	Observed	Simulated	Difference (S − O)	Observed	Simulated	Difference (S − O)
08	220°/18	190°/23	−30°/+5	979.2	979.8	+0.6
07	180°/15	190°/23	+10°/+8	980.9	980.0	−0.9
15	—	190°/21	—/—	984.6	982.3	−2.3
13	176°/18	160°/14	−16°/+4	972.8	976.0	+3.2
11	193°/14	180°/20	−13°/+6	984.3	981.0	−3.3
05	225°/9	230°/12	+5°/+3	988.6	990.2	+1.6
21	202°/6	160°/14	−42°/+8	991.9	989.8	−1.1
Average			−9/+5			−0.5

observed all along the mountain barrier (except at AWS 05), but overall, the pressure pattern is quite well simulated.

In both cases, the blocking effect by Minna Bluff (AWS 05) and the airflow to the east of Ross Island (AWS 08) seem to be well simulated. However, the fact that the model simulated lower pressures along the mountains with respect to the observed (Figs. 13a,b) indicates that the simulated ridging in those areas is less than observed. This may be a consequence of the boundary conditions for the limited domain. Because of the eastern boundary conditions, the strongest winds are along the eastern boundary. In reality, the strongest winds should occur along the mountains. The model does not allow enough flow toward the mountains, and so the model ridging is less than in the real world. However, the model qualitatively simulates the basic flow past a topographic barrier.

b. Discussion

The model best represents cases where the cyclonic forcing causes strong winds directed toward the Transantarctic Mountains over most of the model domain. This gives the dynamics of airflow within one Rossby radius of the mountains, where there is an increase in boundary-layer depth along the mountains. Within this Rossby radius, the cyclonic forcing is not the dominant process (but it is necessary to have the cyclonic forcing driving the flow toward the mountains from the east). When the center of a low is located south of Ross Island, the pressure gradient increases northward along the Transantarctic Mountains, and leeside troughing is expected due to initially ageostrophic downgradient flow. This is observed with strong lows along the south coast of Alaska (Macklin et al. 1988) and may occur along the Transantarctic Mountains near Terra Nova Bay. However, the numerical model has a wall boundary in a restricted domain with strong forcing and results in extreme leeside troughing, which greatly reduces the boundary-layer depth in this region.

We wish to discuss the winds in McMurdo Sound, between Ross Island and the Transantarctic Mountains. The sound is about 50 km wide and 75 km long. The theory of adjustment in straits has been studied by Overland (1984) and applied to the Alaska coast (Lackmann and Overland 1989). For a pressure gradient orthogonal to the strait axis there should be geostrophic flow, while for a pressure gradient parallel to the strait axis there should be gap winds, where the air is accelerated down the pressure gradient toward lower pressure. The minimum time scale for noticeable geostrophic adjustment is a quarter of the inertial period or 3 h at the latitude of Ross Island. This is about the time that it takes an air parcel to travel the length of the sound, and so we might expect some geostrophic adjustment with pressure ridging along the Transantarctic Mountains near the northern part of the sound. However, winds in McMurdo Sound have been inferred from sea-ice observations by O'Connor and Bromwich (1988). The strongest winds are in the eastern part of the sound, along the coast of Ross Island. It appears that the southerly barrier winds are deflected around Mt. Discovery and Minna Bluff and impinge on the south side of Ross Island, with a resulting stagnation zone and pressure increase that causes the flow to split and go around the island. Although most of this flow is to the east of the island, there can be strong winds along the west side as well. For strong barrier wind conditions when the airflow overrides Minna Bluff, there may be a more uniform inflow and the winds might be in geostrophic balance.

From the model and observational results, we can make several conclusions about cyclonically forced barrier wind events along the Transantarctic Mountains.

1) Barrier winds in the vicinity of Minna Bluff and Ross Island primarily result from cyclonic forcing of boundary-layer air toward the Transantarctic Mountains, and this can be modeled by the barotropic dynamics of low-level wind flow encountering steep topography.

2) The boundary-layer depth and resultant surface pressure perturbation increase northward from Byrd Glacier along the mountains.

3) The surface airflow is predominantly to the east of Ross Island, because it must turn around the topography of Mt. Discovery and Minna Bluff. There are flow stagnation regions and resulting local pressure maxima south of Minna Bluff and Ross Island, where the airflow is around these obstacles. The local pressure increase on the south side of Ross Island due to this topographic effect can be as great as 4–6 hPa in a strong barrier wind event.

4) The blocking of the southerly flow by Mt. Discovery/Minna Bluff and Ross Island may contribute to a decrease in the pressure gradient north of Ross Island as a downstream wake effect.

5) The flow through McMurdo Sound is influenced by the blocking effect of orography to the south. The winds at McMurdo Station and in McMurdo Sound should be stronger when surface airflow is over, rather than around, Minna Bluff.

6) Under less stable conditions (case two, judged by the winds and pressures at AWS 18 and 09) the blocking effect may be weaker because some of the boundary-layer air may go over the obstacles (Minna Bluff and Ross Island) instead of around them.

Acknowledgments. This research was supported in part by National Science Foundation Grant DPP 8916921 to David H. Bromwich. We thank the editor, Frederick Sanders, and two anonymous reviewers for their comments. The Institute for Naval Oceanography (INO) was sponsored by the U.S. Naval Research Labs (NRL) and managed by the University Corporation for Atmospheric Research (UCAR) until disestablished on 30 September 1992.

REFERENCES

Allison, I., C. M. Tivendale, G. J. Akerman, J. M. Tann, and R. H. Wills, 1982: Seasonal variations in the surface energy exchanges over antarctic sea ice and coastal waters. *Ann. Glaciol.*, **3**, 12–16.

Bromwich, D. H., 1986: Boundary layer meteorology of the western Ross Sea. *Antarct. J. U.S.*, **21**(5), 237–240.

——, 1987: A case study of mesoscale cyclogenesis over the southwestern Ross Sea. *Antarctic J. U.S.*, **22**(5), 254–256.

——, 1988a: Snowfall in high southern latitudes. *Rev. Geophys.*, **26**, 149–168.

——, 1988b: A satellite study of barrier wind airflow around Ross Island. *Antarct. J. U.S.*, **23**(5), 167–169.

——, 1991: Mesoscale cyclogenesis over the southwestern Ross Sea linked to strong katabatic winds. *Mon. Wea. Rev.*, **119**, 1735–1752.

——, J. F. Carrasco, and C. R. Stearns, 1992: Satellite observations of katabatic wind propagation for great distances across the Ross Ice Shelf. *Mon. Wea. Rev.*, **120**, 1940–1949.

——, Y. Du, and T. R. Parish, 1994: Numerical simulation of winter katabatic winds from West Antarctica crossing Siple Coast and the Ross Ice Shelf. *Mon. Wea. Rev.*, submitted.

Carleton, A. M., 1992: Synoptic interactions between Antarctica and lower latitudes. *Aust. Meteor. Mag.*, **40**, 129–147.

Carrasco, J. F., 1992: A mesoscale cyclogenesis study adjacent to the Pacific coast of Antarctica. M.S. thesis, Atmospheric Sciences Program, The Ohio State University, 179 pp.

——, and D. H. Bromwich, 1993: Mesoscale cyclogenesis dynamics over southwestern Ross Sea. *J. Geophys. Res.*, **98**, 12 973–12 995.

Haltiner, G. J., and R. T. Williams, 1980: *Numerical Prediction and Dynamic Meteorology.* 2d ed., John Wiley and Sons, 477 pp.

Hsu, S. A., 1988: *Coastal Meteorology.* Academic Press, 260 pp.

Keyser, D., and R. A. Anthes, 1977: The applicability of a mixed-layer model of the planetary boundary layer to real-data forecasting. *Mon. Wea. Rev.*, **105**, 1351–1371.

Kozo, T. L., and R. Q. Robe, 1986: Modeling winds and open-water buoy drift along the eastern Beaufort Sea coast, including the effects of the Brooks Range. *J. Geophys. Res.*, **91**, 13 011–13 032.

Lackmann, G. M., and J. E. Overland, 1989: Atmospheric structure and momentum balance during a gap-wind event in Shelikof Strait, Alaska. *Mon. Wea. Rev.*, **117**, 1817–1833.

Lavoie, R. L., 1972: A mesoscale numerical model of lake-effect storms. *J. Atmos. Sci.*, **29**, 1025–1040.

Liu, Z., and D. H. Bromwich, 1993: Acoustic remote sensing of planetary boundary layer dynamics near Ross Island, Antarctica. *J. Appl. Meteor.*, **32**, 1867–1882.

Lu, M., and W. M. Sackinger, 1989: The mountain barrier effect and modification of tabular iceberg motion in a coastal zone. *J. Coastal Res.*, **5**, 701–710.

Macklin, S. A., G. M. Lackmann, and J. Gray, 1988: Offshore-directed winds in the vicinity of Prince William Sound, Alaska. *Mon. Wea. Rev.*, **116**, 1289–1301.

Mass, C. F., and D. P. Dempsey, 1985: A one-level, mesoscale model for diagnosing surface winds in mountainous and coastal regions. *Mon. Wea. Rev.*, **113**, 1211–1227.

——, and M. D. Albright, 1987: Coastal southerlies and alongshore surges of the west coast of North America: Evidence of mesoscale topographically trapped response to synoptic forcing. *Mon. Wea. Rev.*, **116**, 1707–1738.

Mullen, D. P., 1987: Forecasting for the frigid desert of Antarctica. *Weatherwise*, **40**, 304–311.

O'Connor, W. P., and D. H. Bromwich, 1988: Surface airflow around Windless Bight, Ross Island, Antarctica. *Quart. J. Roy. Meteor. Soc.*, **114**, 917–938.

Overland, J. E., 1984: Scale analysis of marine winds in straits and along mountainous coasts. *Mon. Wea. Rev.*, **112**, 2530–2534.

——, 1985: Atmospheric boundary layer structure and drag coefficients over sea ice. *J. Geophys. Res.*, **90**, 9029–9049.

——, 1986: Comments on "Coastal jets in the lower atmosphere." *J. Phys. Oceanogr.*, **16**, 1006.

——, M. H. Hitchman, and Y. J. Han, 1979: A regional surface wind model for mountainous coastal areas. NOAA Tech. Rep. ERL 407-PMEL 32, 34 pp.

——, R. M. Reynolds, and C. H. Pease, 1983: A model of the atmospheric boundary layer over the marginal ice zone. *J. Geophys. Res.*, **88**, 2836–2840.

Parish, T. R., 1983: The influence of the Antarctic Peninsula on the wind field over the western Weddell Sea. *J. Geophys. Res.*, **88**, 2684–2692.

Physick, W. L., 1981: Winter depression tracks and climatological jet streams in the Southern Hemisphere during the FGGE year. *Quart. J. Roy. Meteor. Soc.*, **107**, 883–898.

Savage, M. L., C. R. Stearns, G. Weidner, and D. Fleming, 1985: Antarctic automatic weather station data for the calendar year 1984. Department of Meteorology, University of Wisconsin-Madison, 243 pp. [Available from the Department of Atmospheric and Oceanic Sciences, 1225 W. Dayton St., Madison, WI 53706].

Schwerdtfeger, W., 1984: *Weather and Climate of the Antarctic.* Elsevier, 261 pp.

Shapiro, R., 1970: Smoothing, filtering, and boundary effects. *Rev. Geophys. Space Phys.*, **8**, 359–387.

Slotten, H. R., and C. R. Stearns, 1987: Observations of the dynamics and kinematics of the atmospheric surface layer of the Ross Ice Shelf, Antarctica. *J. Climate Appl. Meteor.*, **26,** 1731–1743.

Taljaard, J. J., 1972: Synoptic meteorology of the Southern Hemisphere. *Meteorology of the Southern Hemisphere,* Meteor. Monogr., No. 13, Amer. Meteor. Soc., 139–213.

Wilczak, J. M., and J. W. Glendening, 1988: Observations and mixed-layer modeling of a terrain-induced mesoscale gyre: The Denver cyclone. *Mon. Wea. Rev.*, **116,** 2688–2711.